Report

Current Biology

MKLP2 Is a Motile Kinesin that Transports the Chromosomal Passenger Complex during Anaphase

Highlights

- MKLP2 is a processive microtubule plus-end directed motor
- CPC is co-transported with MKLP2 and makes it more processive *in vitro*
- MKLP2 and the CPC display directional motility in anaphase
- MKLP2 motor activity specifies CPC localization in anaphase

Authors

Ingrid E. Adriaans, Peter Jan Hooikaas, Amol Aher, ..., Ilya Grigoriev, Anna Akhmanova, Susanne M.A. Lens

Correspondence

a.akhmanova@uu.nl (A. Akhmanova), s.m.a.lens@umcutrecht.nl (S.M.A.L.)

In Brief

In this study, Adriaans, Hooikaas, et al. reconstitute *in vitro* the microtubule-based transport of a major mitotic signaling module, the chromosomal passenger complex (CPC), by the kinesin-6 protein, MKLP2 (KIF20A), and reveal the function of MKLP2 motor activity for CPC localization before the onset of cytokinesis.

Adriaans et al., 2020, Current Biology *30*, 2628–2637
July 6, 2020
https://doi.org/10.1016/j.cub.2020.04.081

CellPress

CellPress
OPEN ACCESS

Current Biology

Report

MKLP2 Is a Motile Kinesin that Transports the Chromosomal Passenger Complex during Anaphase

Ingrid E. Adriaans,[1,2,4] Peter Jan Hooikaas,[3,4] Amol Aher,[3] Martijn J.M. Vromans,[1,2] Robert M. van Es,[1,2] Ilya Grigoriev,[3] Anna Akhmanova,[3,5,*] and Susanne M.A. Lens[1,2,5,6,*]

[1]Oncode Institute, University Medical Center Utrecht, Utrecht University, 3584, Utrecht, the Netherlands
[2]Center for Molecular Medicine, University Medical Center Utrecht, Utrecht University, 3584 Utrecht, the Netherlands
[3]Cell Biology, Neurobiology and Biophysics, Department of Biology, Faculty of Science, Utrecht University, 3584 Utrecht, the Netherlands
[4]These authors contributed equally
[5]Senior author
[6]Lead Contact
*Correspondence: a.akhmanova@uu.nl (A. Akhmanova), s.m.a.lens@umcutrecht.nl (S.M.A.L.)
https://doi.org/10.1016/j.cub.2020.04.081

SUMMARY

During cytokinesis, signals from the anaphase spindle direct the formation and position of a contractile ring at the cell cortex [1]. The chromosomal passenger complex (CPC) participates in cytokinesis initiation by signaling from the spindle midzone and equatorial cortex [2], but the mechanisms underlying the anaphase-specific CPC localization are currently unresolved. Accumulation of the CPC at these sites requires the presence of microtubules and the mitotic kinesin-like protein 2, MKLP2 (KIF20A), a member of the kinesin-6 family [2–7], and this has led to the hypothesis that the CPC is transported along microtubules by MKLP2 [3–5, 7]. However, the structure of the MKLP2 motor domain with its extended neck-linker region suggests that this kinesin might not be able to drive processive transport [8, 9]. Furthermore, experiments in *Xenopus* egg extracts indicated that the CPC might be transported by kinesin-4, KIF4A [10]. Finally, CPC-MKLP2 complexes might be directly recruited to the equatorial cortex via association with actin and myosin II, independent of kinesin activity [4, 8]. Using microscopy-based assays with purified proteins, we demonstrate that MKLP2 is a processive plus-end directed motor that can transport the CPC along microtubules *in vitro*. In cells, strong suppression of MKLP2-dependent CPC motility by expression of an MKLP2 P-loop mutant perturbs CPC accumulation at both the spindle midzone and equatorial cortex, whereas a weaker inhibition of MKLP2 motor using Paprotrain mainly affects CPC localization to the equatorial cortex. Our data indicate that control of cytokinesis initiation by the CPC requires its directional MKLP2-dependent transport.

RESULTS AND DISCUSSION

The Extended Neck and Coiled Coil Domain of MKLP2 Binds to the CPC via the N Termini of INCENP and Borealin

To test the hypothesis that mitotic kinesin-like protein 2 (MKLP2) is a chromosomal passenger complex (CPC)-transporting motor, we first mapped the interaction between them. The CPC consists of INCENP, Survivin, Borealin, and Aurora B [11], and previous work suggested that the C-terminal half of MKLP2 binds the N terminus of INCENP [7, 12]. We generated several GFP-tagged fragments of MKLP2 and INCENP, expressed these in mitotic HEK293T cells, and assessed their ability to immunoprecipitate endogenous CPC or MKLP2, respectively (Figures 1A, 1B, and S1A–S1C). Although cyclin B-Cdk1-dependent phosphorylation of either INCENP or MKLP2 is thought to interfere with CPC-MKLP2 binding [7, 12], we consistently co-immunoprecipitated endogenous CPC with MKLP2::GFP, as well as endogenous MKLP2 with INCENP::GFP from these mitotic extracts (Figures S1A–S1C). In mitotic cells, a fraction of (overexpressed) INCENP and MKLP2 might not be phosphorylated, and this could be the fraction we pulled down.

Interaction with the CPC depended on a small MKLP2 region (amino acids [aas] 513–765), composed of the extended kinesin neck and coiled coil domain (Figures 1A and S1A). A recombinant N-terminal fragment of INCENP (aas 1–58; referred to as CEN-box; essential for centromere targeting of the CPC via Borealin and Survivin) [13–16] has been shown to interact with recombinant MKLP2 [12]. However, we found that INCENP 1–63 did not efficiently bind endogenous MKLP2, although a somewhat longer N-terminal fragment of INCENP (aas 1–100) bound MKLP2 more efficiently (Figures 1B and S1B). We therefore conclude that there are additional interactions between MKLP2 and INCENP outside the CEN-box. Deletion of the first 48 aas of INCENP (INCENP 49–918), which severely impaired INCENP interaction with Borealin and Survivin (Figures 1B and S1C) [13, 14, 17], reduced the binding to endogenous MKLP2 as compared to full-length INCENP (Figure S1C), suggesting a

CellPress
OPEN ACCESS

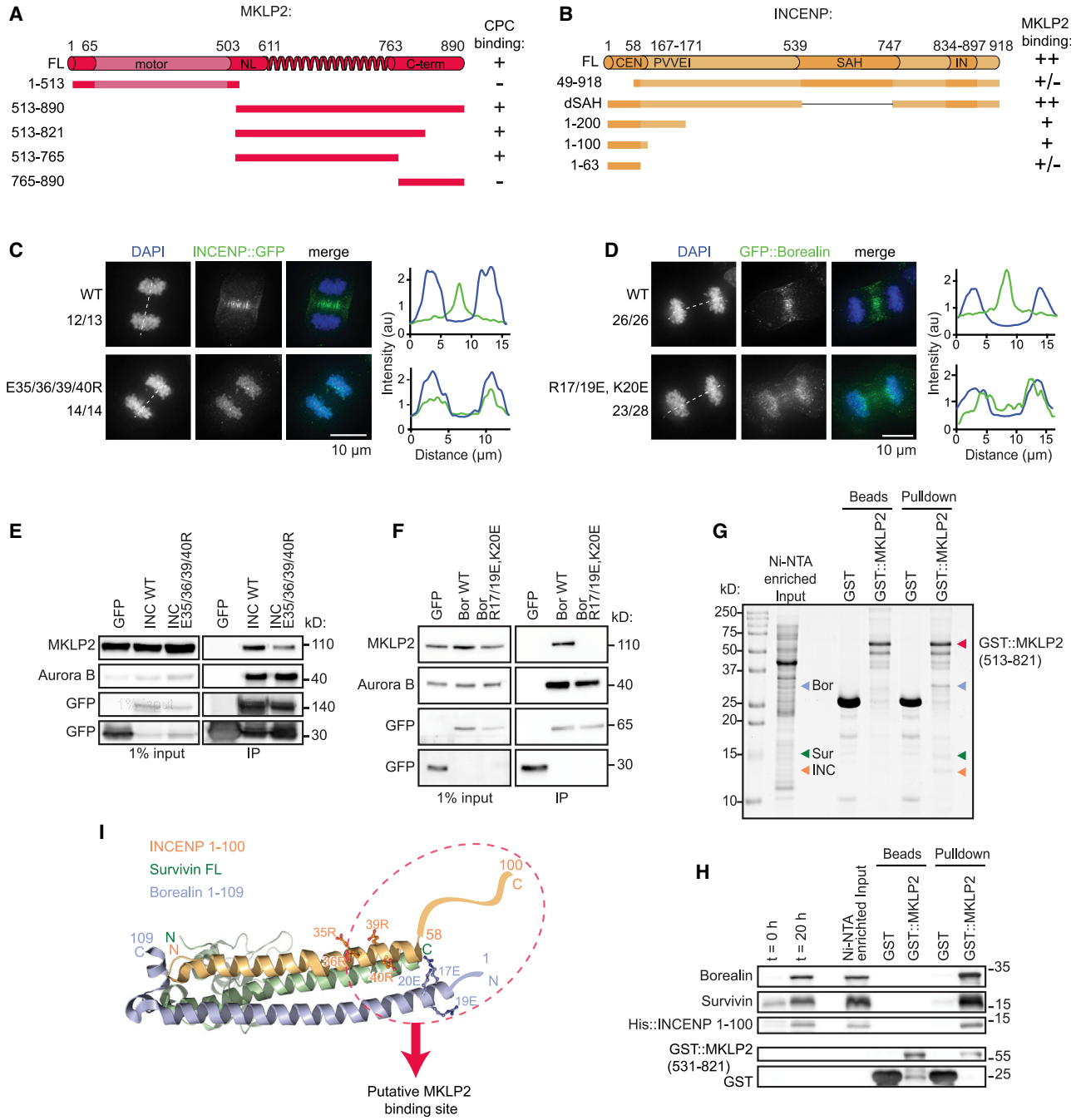

Figure 1. The Extended Neck and Coiled Coil Domain of MKLP2 Binds to the CPC via the N Termini of INCENP and Borealin

(A) Cartoon of full-length (FL) human MKLP2 protein and used MKLP2 fragments. C-term, C-terminal domain; motor, motor domain; NL, neck linker region. Their ability to pull down detectable amounts of endogenous CPC (Figure S1A) is indicated.

(B) Cartoon of human INCENP and used INCENP deletion mutants. CEN, centromere-targeting domain interacting with Borealin and Survivin; IN, IN box interacting with Aurora B; PVVEI, HP1 binding motif; SAH, single α helix. Their ability to pull down detectable amounts of endogenous MKLP2 (Figures S1B and S1C) is indicated.

(C and D) IF for GFP of HeLa cells expressing INCENP::GFP or INCENP E35/36/39/40R::GFP (C) or expressing GFP::Borealin or GFP::Borealin R17/19E, K20E (D). DNA is visualized by DAPI. Dotted line indicates line scan position for GFP and DAPI shown on the right. The number of times the depicted localization was observed/total number of imaged cells is indicated.

(E and F) HEK293T cells were transfected with plasmids encoding: GFP, INCENP WT::GFP or E35/36/39/40R::GFP (E) and GFP, GFP::Borealin WT or R17/19E, K20E (F). Immunoprecipitations were performed with GFP-Trap beads. Samples were analyzed by western blotting.

(G) Coomassie-stained SDS-PAGE gel of a pull-down assay with GST and GST::MKLP2 513-821 (red arrowhead). The CPC components expressed from a tricistronic vector containing 6xHis::INCENP 1–100 (orange), Survivin (green), and Borealin (blue) were enriched from the input lysate using Ni-NTA beads.

(legend continued on next page)

potential contribution of Borealin and/or Survivin to the interaction with MKLP2. To further define CPC-MKLP2 interaction sites, we mutated a conserved set of exposed glutamic acids in the N terminus of INCENP to positively charged residues (E35/36/39/40R) or mutated several positively charged residues in the N terminus of Borealin to negatively charged residues (R17/19 and K20E). These mutations do not interfere with the interactions between CPC members [13] but do perturb the translocation of the CPC from chromosomes in (pro)metaphase to the spindle midzone in anaphase, very similar to what is seen after knockdown of MKLP2 [4, 5, 7, 13] (Figures 1C, 1D, and S1D). The INCENP E35/36/39/40R mutant was less efficient, and the Borealin R17/19, K20E mutant was deficient in precipitating MKLP2 compared to their wild-type counterparts (Figures 1E and 1F). Finally, glutathione S-transferase (GST)::MKLP2 513–821 purified from bacteria, precipitated 6xHis::INCENP 1–100, Borealin, and Survivin expressed in bacteria (Figures 1G and 1H). This strongly suggests that the interaction between the non-enzymatic CPC core members and MKLP2 is direct.

INCENP 1–58, Borealin 10–109, and Survivin form a three-helix bundle structure *in vitro* [13]. Based on this structure, the residues of INCENP and Borealin involved in MKLP2 binding are clustered on one side of the three-helix bundle (Figure 1I). Moreover, aas 63–100 of INCENP would be oriented toward the N terminus of Borealin, and together, they could form the interface for binding MKLP2. Whether Survivin also makes direct contacts with MKLP2 is currently unclear; it may contribute to MKLP2 binding by participating in the formation of the three-helix bundle with INCENP and Borealin.

MKLP2 Is a Motile Kinesin that Becomes More Processive in the Presence of the CPC

Next, we investigated whether MKLP2 can transport the CPC by using *in vitro* reconstitution assays in combination with total internal reflection fluorescence (TIRF) microscopy. In these assays, dynamic microtubules were grown from GMPCPP-stabilized microtubule seeds that are attached to a glass coverslip [18, 19]. Imaging was performed using fluorescently labeled proteins and (un)labeled tubulin [20]. Full-length GFP-tagged human MKLP2 (MKLP2::GFP) was purified from HEK293T cells using StrepII-tag affinity purification (Figure S2A). Fluorescence intensity measurements of single MKLP2::GFP molecules showed they were homodimers (Figure S2B). Mass spectrometry analysis revealed MKLP2 as the main protein in the elution, although some contaminants were present. Notably, a few KIF4A peptides were detected, but intensity-based quantification estimated the KIF4A abundance to be at least 9,000 times less than that of MKLP2 (Figure S2C). We used a similar approach to purify GFP::StrepII- or mCherry::StrepII-tagged human CPC, but the complex containing full-length INCENP was highly unstable. We therefore generated a recombinant "coreCPC" consisting of full-length Survivin and Borealin with INCENP(1–100)::GFP/mCherry (Figures 2A and S2D). In addition, we also generated a complex that contained full-length Survivin, Borealin, and INCENP(1–100)-linker-INCENP(834–918)::GFP/mCherry. Because INCENP(834–918) interacts with Aurora B [21, 22], it could be loaded with a wild-type (WT) or kinase-dead (KD) variant of Aurora B (Figures 2A, S2E, and S2F). We refer to this complex as "miniCPC." Aurora B kinase activity in miniCPC containing WT Aurora B, but not the KD mutant, was confirmed by an *in vitro* kinase assay (Figure S2G).

Single MKLP2::GFP molecules exhibited plus-end directed movement on microtubules with an average run length of 1.1 ± 1.2 μm and a velocity of 0.15 ± 0.05 μm/s (Figures 2B–2D and S2H–S2J). Importantly, this velocity differs from that of the mouse (0.92 ± 0.15 μm/s) and *X. laevis* (0.8 μm/s) KIF4A homologs [23, 24], making it highly unlikely that the observed motility was caused by co-purified KIF4A. In fact, similar to *C. elegans* MKLP1 (KIF23; ~0.2 μm/s), MKLP2 is relatively slow compared to other processive kinesins (e.g., KIF1A, KIF5B, and KIF21A/B), which all move at velocities higher than 0.5 μm/s [20, 25–27]. In the presence of mCherry-tagged coreCPC, MKLP2::GFP became more processive with an increased run length of 1.5 ± 1.6 μm (Figures 2B, 2C, and S2I). This value might be an underestimation because it is based on the analysis of "complete" motor tracks, where both landing and dissociation of the motor were observed, and does not include "incomplete" tracks. In addition, coreCPC negatively affected the landing frequency of MKLP2::GFP although velocities remained unchanged (Figures 2B, 2D, and S2K).

Next, we assayed the influence of Aurora B on MKLP2::GFP motility using mCherry-tagged miniCPC complexes, with either WT or KD Aurora B. Although coreCPC caused a modest increase of MKLP2::GFP processivity by 48.3%, the presence of miniCPC made MKLP2::GFP motors hyperprocessive. For most tracks, no start and/or end point could be detected, and run length could thus not be determined (Figures 2E and 2F). Furthermore, MKLP2::GFP velocity was decreased to 0.08 ± 0.03 μm/s by miniCPC(WT) and 0.10 ± 0.04 μm/s by miniCPC(KD), respectively (Figures 2E, 2G, and S2L). Importantly, Aurora B kinase activity had no clear effect on any measured motility parameter, as miniCPC(KD) showed similar effects as miniCPC(WT) (Figures 2E–2G, S2L, and S2M). Thus, MKLP2 is a motile kinesin that displays increased processivity in the presence of CPC, irrespective of Aurora B kinase activity.

MKLP2 Transports the CPC along Microtubules *In Vitro*

In the absence of MKLP2, both core- and miniCPC showed some binding and diffusive behavior on microtubules *in vitro*. Because the microtubule binding SAH (single α helix) domain of INCENP is not present in our recombinant complexes [15, 16, 28–30], their ability to interact with microtubules most likely involves Borealin and the N terminus of INCENP, in line with the fact that both co-pellet with microtubules *in vitro* [31, 32]. Interestingly, the miniCPC bound microtubules significantly better than coreCPC (Figures 2H–2J), suggesting that the INCENP C

(H) Western blots of a pull-down with GST and GST-tagged MKLP2 513-821 probed with the indicated antibodies. Time points indicate inputs of bacterial lysates before and after IPTG induction.

(I) Ribbon representation of the 3-helix-bundle structure of the CPC core complex, consisting of INCENP (aas 1–58), Borealin (aas 10–109), and Survivin (aas 1–140) [13] with amino acid side chains E35/36/39/40 in INCENP and R17/19, K20 in Borealin indicated (PDB: 2QFA). The hypothetical location of the C-terminal aas 59–100 of INCENP and N-terminal aas 1–9 of Borealin is added to the crystal structure.

CellPress
OPEN ACCESS

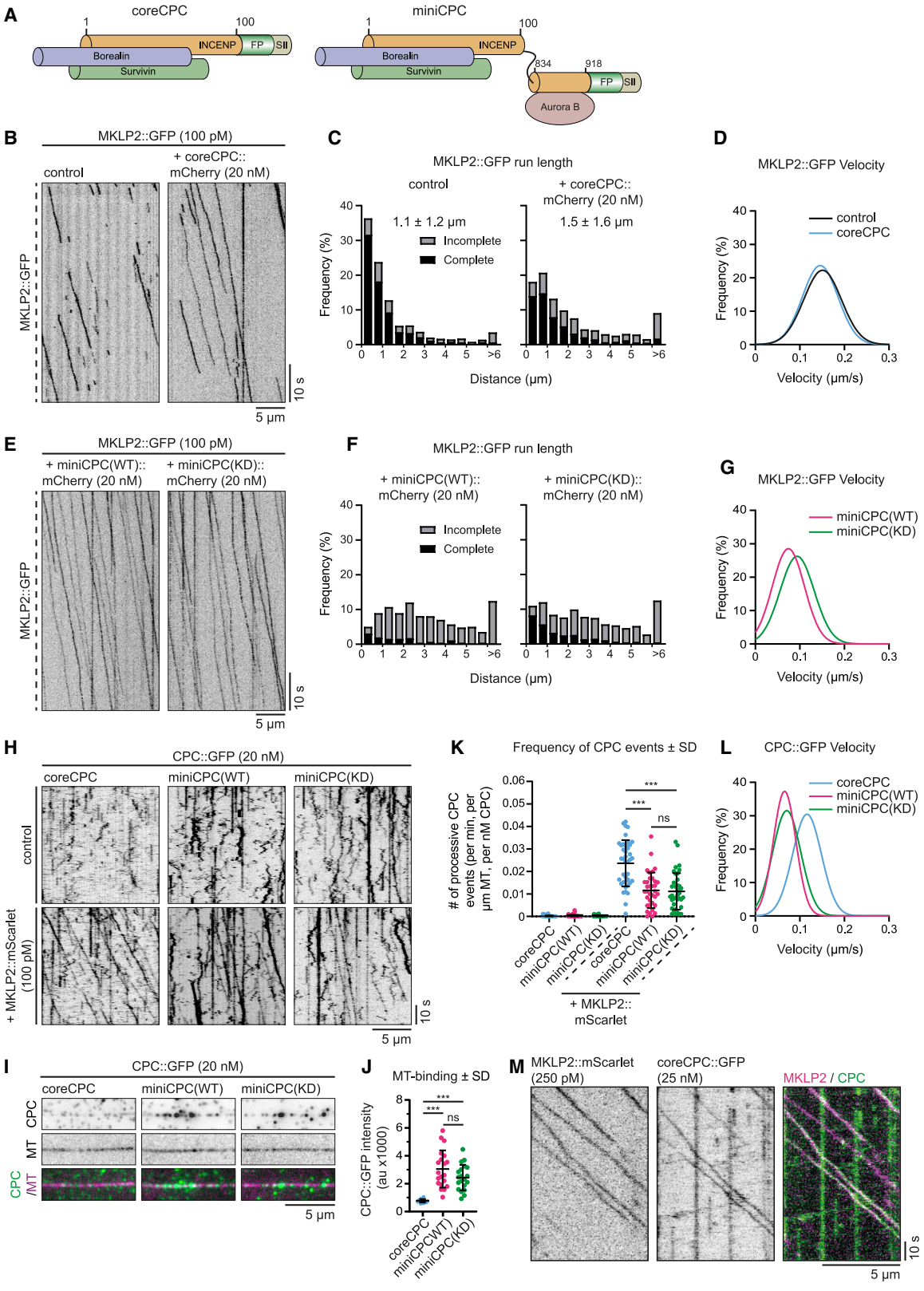

Figure 2. MKLP2 Is a Motile Motor that Transports CPC Complexes *In Vitro*

(A) Cartoons of purified coreCPC and miniCPC complexes. FP, fluorescent protein (GFP or mCherry); SII, StrepII-tag.

(B) Representative kymographs of MKLP2::GFP on dynamic microtubules. Image acquisition: 10 frames per second (fps).

(legend continued on next page)

terminus together with Aurora B increases microtubule binding affinity of the complex. Addition of MKLP2::mScarlet to both core- and miniCPC induced processive plus-end directed movement of CPC on microtubules (Figures 2H, 2K, and S2A). CoreCPC movement was seen more frequently than that of miniCPC, although Aurora B activity again did not seem to affect motility (Figures 2H and 2K). In agreement with the observation that miniCPC, but not coreCPC, slowed down MKLP2::GFP (Figures 2D and 2G), miniCPC::GFP moved at a lower velocity (WT: 0.07 ± 0.03 μm/s; KD: 0.08 ± 0.03 μm/s) compared to coreCPC::GFP (0.11 ± 0.03 μm/s) in the presence of MKLP2::mScarlet (Figures 2L and S2N). These data suggest that the interaction of miniCPC with microtubules promotes processivity of an MKLP2-CPC complex at the expense of velocity. Finally, using dual-color TIRF imaging, we confirmed that MKLP2 tracks correspond to those of moving coreCPC on a single microtubule (Figure 2M). In summary, we show that MKLP2 is a motile kinesin capable of transporting a CPC complex along microtubules *in vitro*.

MKLP2 and INCENP Display Directional Motility toward the Midzone and Equatorial Cortex in Anaphase Cells

To investigate whether MKLP2 and CPC also show directional motility in cells, we analyzed HeLa cells stably expressing either MKLP2::GFP or INCENP::GFP (Figures S3A–S3E) [29]. Live-cell imaging during anaphase revealed the presence of discrete particles labeled with MKLP2::GFP or INCENP::GFP (Figures 3A and 3B; Videos S1 and S2). In line with previous work [8], we found that the majority of particles showed diffusive behavior or remained static. However, motile events displaying clear directionality were also observed (Figures 3A and 3B; Videos S1 and S2). Quantification of unidirectional events with a duration >2.5 s and a velocity >0.05 μm/s revealed that the majority of these events (59% for MKLP2::GFP; 54% for INCENP::GFP) were oriented toward the equatorial cortex (magenta tracks). Co-expression of β-tubulin::Halo showed that MKLP2::GFP punctae were present on microtubules directed toward the equatorial cortex (Figure 3C). Some of these punctae could correspond to protein localization to growing microtubule ends as described for *D. melanogaster* Aurora B [33]. Motile events directed toward the spindle midzone (orange tracks) constituted 28% (MKLP2) and 33% (INCENP) of all directional tracks. This may be an underestimation because molecular crowding in the midzone area made it more difficult to discern motile events. The remaining tracks showed no preferred direction (Figures 3A, 3B, 3D, and 3E; Videos S1 and S2). Strikingly, the directional MKLP2 and INCENP events had similar velocities of 0.19 ± 0.05 μm/s and 0.19 ± 0.06 μm/s, respectively (Figures 3F, S3F, and S3G). The MKLP2 and INCENP velocities in cells were slightly higher compared to those measured *in vitro* (Figures 2D, 2G, 2L, S2J, S2L, and S2N), possibly because our *in vitro* assays were performed at 30°C, whereas cell culture experiments were carried out at 37°C. Furthermore, the influence of additional cellular factors on velocity cannot be ruled out. In short, we show that MKLP2 and INCENP show not only diffusive [8] but also directional motility in cells during anaphase.

MKLP2 Motor Activity Specifies CPC Localization in Anaphase

To test whether MKLP2-mediated transport is involved in CPC localization in anaphase, we used two approaches to perturb MKLP2 motor activity. First, we generated a P-loop mutation (T167N), conserved among all kinesin families and described to lock kinesin-1 in a strong microtubule-binding ("rigor") state [34] (Figures S4A and S4B). Second, we made use of Paprotrain, an MKLP2-specific non-competitive ATPase inhibitor, which does not affect KIF4A and the two MKLP2-related kinesin-6 motors, MKLP1 and MPP1 (KIF20B) [35]. MKLP2 *in vitro* motility on dynamic microtubules was blocked by the T167N mutation and severely reduced by 50 μM Paprotrain (Figure 4A). Although WT and T167N motors showed similar microtubule-binding efficiencies, the addition of Paprotrain reduced the number of motors landing on microtubules by 50% (Figure 4B). Moreover, MKLP2 dwell time was reduced from 8.5 ± 9.3 s (WT) to 3.7 ± 4.1 s (T167N) and 3.1 ± 4.2 s (Pap; Figures 4C and S4C). Thus, MKLP2 T167N does not exhibit "rigor"-like, microtubule binding but is impaired in movement with an increased off rate. Paprotrain showed a dose-dependent effect on MKLP2 motility parameters; run length, landing frequency, and velocity were reduced at increasing Paprotrain concentrations (Figures S4D–S4H). Furthermore, 47% of motors were static in the presence of 50 μM Paprotrain (Figures 4A, S4D, and S4I). The capacity of T167N and Paprotrain-treated MKLP2::mScarlet motors to recruit coreCPC::GFP complexes to microtubules *in vitro* was reduced by 50% and 56%, respectively, compared to WT MKLP2 (Figures 4D and 4E). Furthermore, most coreCPC complexes were stalled in the presence of the T167N

(C) Histograms of MKLP2::GFP run length. Complete tracks: both landing and dissociation of the motor were observed. Incomplete tracks: tracks exceed the 90-s acquisition time or partially took place outside the acquisition area. Average run length ± standard deviation (SD) of complete tracks is indicated (Figure S2I); n = 1,145 and 1,137 kinesins from three experiments.
(D) Gaussian fits of MKLP2::GFP velocities. Histograms are in Figure S2J.
(E) Representative kymographs of MKLP2::GFP on dynamic microtubules in the presence of miniCPC::mCherry with active (WT) or inactive (kinase-dead [KD]) Aurora B. Image acquisition: 10 fps.
(F) Histograms of MKLP2::GFP run length in the presence of miniCPC::mCherry. n = 459 and 657 kinesins from two experiments.
(G) Gaussian fits of MKLP2::GFP velocities in the presence of miniCPC. Histograms are in Figure S2L.
(H) Kymographs of core- and miniCPC::GFP on dynamic microtubules ± MKLP2::mScarlet. Image acquisition: 4 fps.
(I) Representative images showing core- or miniCPC on dynamic rhodamine-labeled microtubules.
(J) Quantification of core- and CPC::GFP intensities on dynamic microtubules. n = 20 microtubules/condition. ***$p < 0.001$ (t test). Error bars denote SD.
(K) Quantification of processive CPC events per microtubule normalized for microtubule length, time of acquisition, and CPC concentration. n = 44, 48, 47, 40, 35, and 37 microtubules from three experiments. ***$p < 0.001$ (Mann-Whitney *U* test). Error bars denote SD.
(L) Gaussian fits of core- and miniCPC::GFP velocities. Histograms are in Figure S2N.
(M) Kymographs of dual-color *in vitro* reconstitution experiments with MKLP2::mScarlet and coreCPC::GFP. Image acquisition: 2 fps.

CellPress
OPEN ACCESS

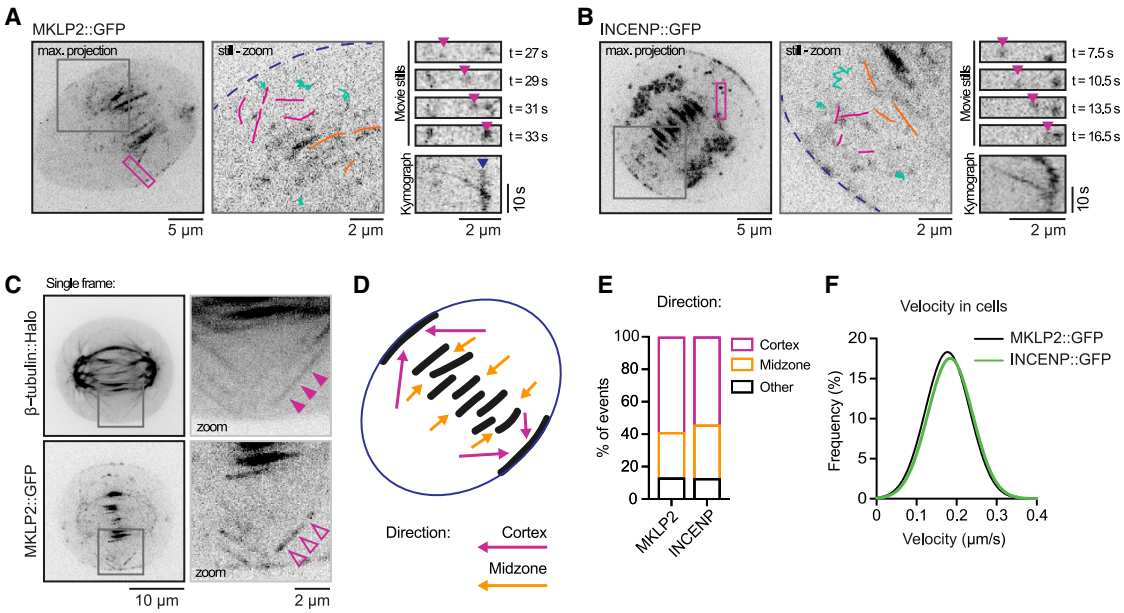

Figure 3. MKLP2 and INCENP Display Directional Motility in Cells

(A and B) Maximum intensity projections and corresponding zooms of HeLa cells in anaphase expressing MKLP2::GFP (A; Video S1; Figures S3A and S3C) or INCENP::GFP (B; Video S2; Figure S3B). A number of representative particles were traced and categorized as non-directional (diffusive or static, turquoise) or directional toward the equatorial cortex (magenta) or the spindle midzone (orange). Blue dotted line in zoom indicates the cell cortex. Panels on the right (magenta box in max. projection) are stills of different time points and corresponding kymograph of a directional event (magenta arrowheads) going toward the equatorial cortex (blue arrowhead). Note that ectopically expressed INCENP::GFP was frequently detected on chromatin in anaphases of otherwise untreated cells. See also [8].

(C) Representative stills and corresponding zooms of a HeLa cell in anaphase expressing MKLP2::GFP and co-transfected with β-tubulin::Halo. Microtubules were visualized by fluorescent TMR ligand. Zooms show a microtubule close to the cell cortex (solid arrowheads) positive for MKLP2::GFP (open arrowheads).

(D) Cartoon of an anaphase cell with spindle midzone and equatorial cortex in black and arrows displaying the two main orientations of directional MKLP2::GFP and INCENP::GFP motility events: toward the equatorial cortex (magenta) and midzone (orange).

(E) Quantification of MKLP2::GFP and INCENP::GFP particle directionality. n = 107 events from 32 cells (MKLP2) and n = 94 events from 19 cells (INCENP).

(F) Gaussian fits of MKLP2::GFP (black) and INCENP::GFP (green) velocities. Histograms are shown in Figures S3F and S3G.

mutant (Figures 4F and 4G), whereas the addition of 50 μM Paprotrain reduced the number of transport events as well as the velocity of moving coreCPC complexes (Figures 4F, 4G, S4J, and S4K).

We subsequently knocked down endogenous MKLP2 by small interfering RNA (siRNA) in HeLa cell lines expressing MKLP2(T167N)::GFP or WT MKLP2::GFP (Figures 4H, S3A, and S3C). Similar to WT MKLP2::GFP, MKLP2(T167N)::GFP was cytosolic in metaphase (Figure S3H). However, in anaphase, MKLP2(T167N)::GFP decorated the entire anaphase spindle instead of localizing to the spindle midzone and equatorial cortex (Figure 4H). Endogenous CPC (detected by immunofluorescence [IF] for Aurora B) followed the alternative localization of MKLP2(T167N)::GFP in anaphase (Figure 4H). MKLP2(T167N)::GFP thus allows the relocation of the CPC from chromosomes to anaphase spindle microtubules, but in the absence of motor activity, the CPC fails to concentrate at the spindle midzone and equatorial cortex.

Addition of 50 μM Paprotrain 50 min after release from a Cdk1 inhibitor block also allowed the relocation of either MKLP2 and CPC from the chromosomes to the anaphase spindle (Figures 4I, upper panel, and 4J). However, MKLP2 and CPC were absent from the equatorial cortex, visualized by staining for Anillin (Figures 4I, middle panel, and 4J), and their localization on the spindle midzone, visualized by staining for PRC1, was reduced and more dispersed (Figures 4I and 4J). Similarly, live-cell imaging of INCENP::GFP revealed that, in the majority of the Paprotrain-treated cells, the midzone pool of INCENP::GFP was detectable but somewhat more dispersed (Figures 4K and S3I; Videos S3 and S4), whereas the cortical pool of INCENP::GFP was hardly detectable (Figures 4K, 4L, and S3I). Importantly, localization of the microtubule crosslinker PRC1, which concentrates on the antiparallel microtubule overlaps in the anaphase spindle midzone [24, 36–38], was unchanged (Figure 4I, lower panel). This most likely explains why Paprotrain addition at this time point did not impair cleavage furrow ingression (Figures S3I and S3J; Videos S3 and S4) and hardly affected the completion of cytokinesis (Figure S3K), as spindle midzone-derived signals can induce cytokinesis even when MKLP2 is absent or Aurora B inhibited [2, 39, 40]. Taken together, strong suppression of MKLP2-dependent CPC motility with the T167N mutant perturbs CPC accumulation at both the spindle midzone and equatorial cortex, whereas a weaker inhibition of MKLP2 motor using Paprotrain mainly affects CPC localization to the equatorial cortex.

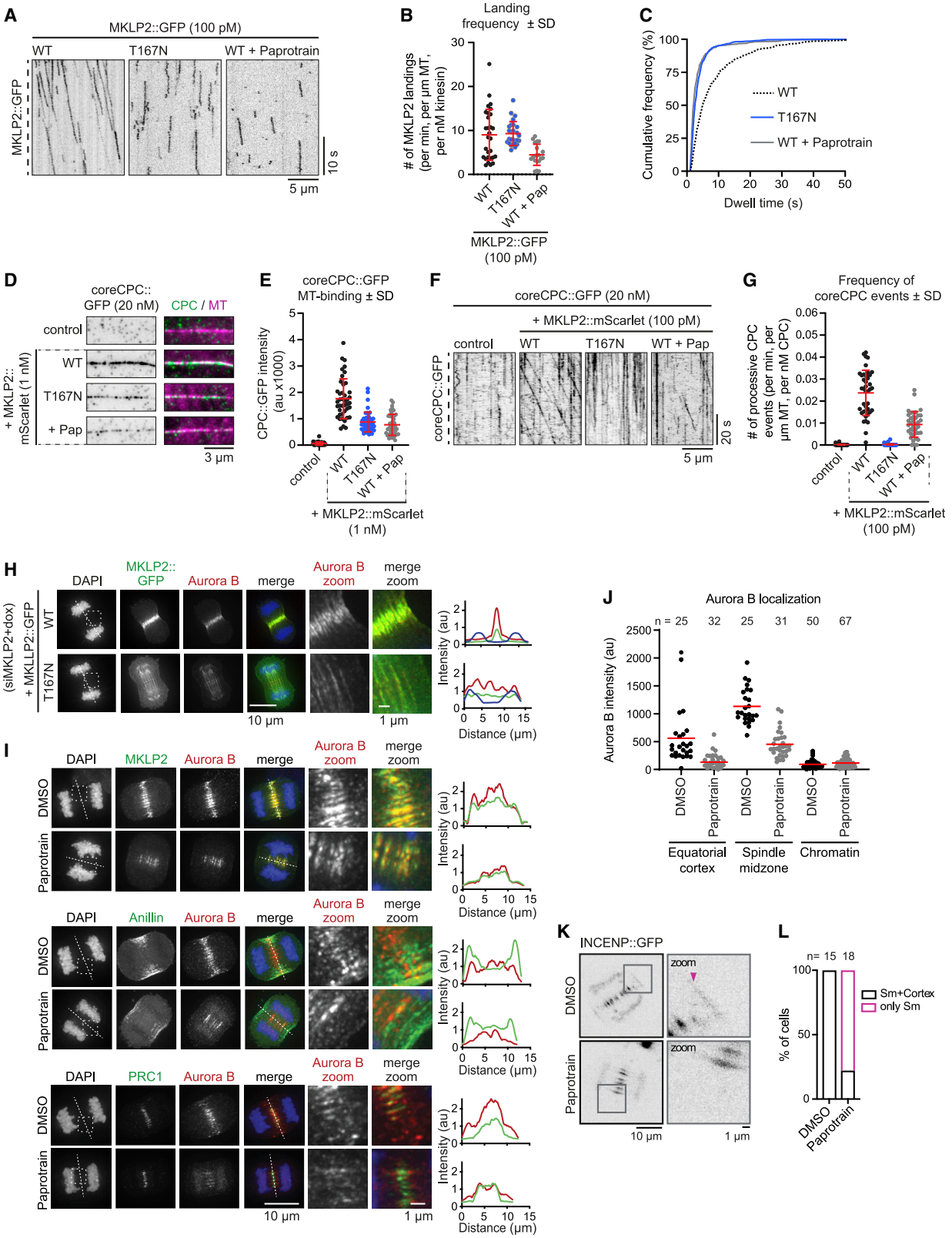

Figure 4. Inhibition of MKLP2 Activity Perturbs CPC Localization in Anaphase

(A) Representative kymographs of WT, T167N, and 50 µM Paprotrain-treated MKLP2::GFP on dynamic microtubules. Image acquisition: 10 fps. Quantifications of different motor properties are in Figures S4D–S4I.

(legend continued on next page)

Conclusions

Our combined *in vitro* and cell-based experiments indicate that MKLP2 functions as a processive motor that focuses the CPC at the antiparallel microtubule overlaps of the anaphase spindle midzone and transports the CPC along microtubules toward the equatorial cortex. The MKLP2-CPC complex might subsequently dock at the cell cortex through interactions with myosin II and actin [4, 8]. Despite the fact that the motor domain of MKLP2 has an atypical structure and mechanochemistry [9], full-length MKLP2 can move processively along microtubules. Furthermore, our *in vitro* reconstitution experiments suggest that the interaction with the CPC promotes processivity of MKLP2 at the expense of its velocity and independently of Aurora B kinase activity. This property is likely caused by direct interactions of different CPC components with microtubules [15, 16, 28, 29, 31, 32], although some effects on the conformation of the MKLP2 molecule may also be involved. Because miniCPC, used in our experiments, lacks the microtubule binding SAH domain of INCENP, we cannot exclude that, in the presence of full-length INCENP, motor velocity is further reduced. However, we deem it unlikely that MKLP2 is stalled by binding to full-length CPC in cells, as both MKLP2 and INCENP exhibit directional motility with similar velocities in cells. Because of the differences in ionic strength, temperature, and molecular crowding in cells versus the *in vitro* conditions, it is possible that MKLP2 by itself would move in cells faster than in our *in vitro* assays and that the CPC slows it down in cells, similar to what we observed *in vitro*. Why only a subset of MKLP2-CPC complexes moves directionally in cells is currently unclear. Post-translational modification of MKLP2, the CPC, or microtubules or the presence of specific microtubule-associated proteins may control the motility of MKLP2-CPC complexes or their preference for specific microtubule tracks. Overall, our data provide a mechanistic basis for the anaphase-specific CPC accumulation at the spindle midzone and equatorial cortex.

STAR★METHODS

Detailed methods are provided in the online version of this paper and include the following:

SUPPLEMENTAL INFORMATION

Supplemental Information can be found online at https://doi.org/10.1016/j.cub.2020.04.081.

ACKNOWLEDGMENTS

We thank Drs. M. Glotzer, S. Wheatley, and T. Stukenberg for their generous gift of reagents; Dr. M. Hadders for his help with Figure 1I; and Dr. H.R. Vos for proteomics support. This work is financially supported by the Netherlands Organisation for Scientific Research, the Netherlands (NWO-Vici 91812610 to S.M.A.L. and NWO ALW Open Program grant 824.15.017 to A.Akhmanova). Proteomics was supported by the Proteins at Work Initiative, the Netherlands (NWO 184.032.201). The group of S.M.A.L. is part of Oncode Institute, which is partly financed by the Dutch Cancer Society, the Netherlands.

(B) Quantification of MKLP2::GFP landing frequency normalized for microtubule length, time of acquisition, and kinesin concentration. n = 29, 26, and 20 microtubules from two or three experiments. Error bars denote SD.
(C) Cumulative frequency plot of dwell times. n = 845 (WT), 929 (T167N), and 336 (WT+Paprotrain) kinesins from two or three experiments.
(D) Representative images showing coreCPC::GFP on dynamic rhodamine-labeled microtubules *in vitro*.
(E) Quantification of coreCPC::GFP intensities on dynamic microtubules. n = 42, 42, 47, and 45 microtubules from two experiments.Error bars denote SD.
(F) Representative kymographs of coreCPC::GFP on dynamic microtubules. Image acquisition: 4 fps.
(G) Quantification of processive coreCPC events per microtubule normalized for microtubule length, time of acquisition, and coreCPC concentration. n = 58, 40, 58, and 38 microtubules from two or three experiments. Error bars denote SD. Data points for MKLP2 WT correspond to Figure 2K.
(H) Representative IF images of HeLa cells expressing MKLP2::GFP or MKLP2 (T167N)::GFP (Figures S3A and S3C). Endogenous MKLP2 was depleted by siRNA (Figures S3D and S3E). Anaphase cells were stained for GFP and Aurora B, DNA by DAPI. Dotted box and line in DAPI indicates respectively zoom area and position of the line scan shown on the right. MKLP2::GFP (green), Aurora B (red), and DAPI (blue) are shown.
(I) Representative IF images of anaphase HeLa cells minus (DMSO) or plus 50 μM Paprotrain (10 min treatment; fixation 60 min after Cdk1 inhibitor release). Dotted box and line in DAPI indicates, respectively, zoom area and position of the line scan shown on the right for, respectively, MKLP2, Anillin, and PRC1 (green) with Aurora B (red).
(J) Quantification of Aurora B intensity levels on the equatorial cortex, the spindle midzone, and on chromatin in anaphase cells treated with either DMSO or 50 μM Paprotrain. n, number of cells analyzed. Red bars represent mean values.
(K) Representative stills (corresponds to 02:30 [DMSO] and 03:00 [Paprotrain] of Figure S3I and Videos S3 and S4) with zooms of HeLa cells expressing INCENP::GFP. Paprotrain (50 μM) or DMSO was added after Cdk1 inhibitor release. Arrowhead indicates cortical localization.
(L) Percentage of living cells showing spindle midzone (Sm) or Sm plus cortical localization of INCENP::GFP.

AUTHOR CONTRIBUTIONS

I.E.A. and S.M.A.L. conceived the project. I.E.A., P.J.H., A.Akhmanova, and S.M.A.L. designed the experiments. I.E.A., P.J.H., A. Aher, M.J.M.V., R.M.v.E., and I.G. performed the experiments. I.E.A. and P.J.H. analyzed the experiments. I.E.A., P.J.H., A.Akhmanova, and S.M.A.L. wrote, reviewed, and edited the manuscript. S.M.A.L. and A.Akhmanova supervised the project.

DECLARATION OF INTERESTS

The authors declare no competing interests.

Received: September 16, 2019
Revised: March 20, 2020
Accepted: April 28, 2020
Published: June 4, 2020

REFERENCES

1. Green, R.A., Paluch, E., and Oegema, K. (2012). Cytokinesis in animal cells. Annu. Rev. Cell Dev. Biol. *28*, 29–58.
2. Adriaans, I.E., Basant, A., Ponsioen, B., Glotzer, M., and Lens, S.M.A. (2019). PLK1 plays dual roles in centralspindlin regulation during cytokinesis. J. Cell Biol. *218*, 1250–1264.
3. Murata-Hori, M., and Wang, Y.L. (2002). Both midzone and astral microtubules are involved in the delivery of cytokinesis signals: insights from the mobility of aurora B. J. Cell Biol. *159*, 45–53.
4. Kitagawa, M., Fung, S.Y.S., Onishi, N., Saya, H., and Lee, S.H. (2013). Targeting aurora B to the equatorial cortex by MKlp2 is required for cytokinesis. PLoS ONE *8*, e64826.
5. Gruneberg, U., Neef, R., Honda, R., Nigg, E.A., and Barr, F.A. (2004). Relocation of aurora B from centromeres to the central spindle at the metaphase to anaphase transition requires MKlp2. J. Cell Biol. *166*, 167–172.
6. Cesario, J.M., Jang, J.K., Redding, B., Shah, N., Rahman, T., and McKim, K.S. (2006). Kinesin 6 family member Subito participates in mitotic spindle assembly and interacts with mitotic regulators. J. Cell Sci. *119*, 4770–4780.
7. Hümmer, S., and Mayer, T.U. (2009). Cdk1 negatively regulates midzone localization of the mitotic kinesin Mklp2 and the chromosomal passenger complex. Curr. Biol. *19*, 607–612.
8. Landino, J., Norris, S.R., Li, M., Ballister, E.R., Lampson, M.A., and Ohi, R. (2017). Two mechanisms coordinate the recruitment of the chromosomal passenger complex to the plane of cell division. Mol. Biol. Cell *28*, 3634–3646.
9. Atherton, J., Yu, I.-M., Cook, A., Muretta, J.M., Joseph, A., Major, J., Sourigues, Y., Clause, J., Topf, M., Rosenfeld, S.S., et al. (2017). The divergent mitotic kinesin MKLP2 exhibits atypical structure and mechanochemistry. eLife *6*, e27793.
10. Nguyen, P.A., Groen, A.C., Loose, M., Ishihara, K., Wühr, M., Field, C.M., and Mitchison, T.J. (2014). Spatial organization of cytokinesis signaling reconstituted in a cell-free system. Science *346*, 244–247.
11. van der Horst, A., and Lens, S.M.A. (2014). Cell division: control of the chromosomal passenger complex in time and space. Chromosoma *123*, 25–42.
12. Kitagawa, M., Fung, S.Y.S., Hameed, U.F.S., Goto, H., Inagaki, M., and Lee, S.H. (2014). Cdk1 coordinates timely activation of MKlp2 kinesin with relocation of the chromosome passenger complex for cytokinesis. Cell Rep. *7*, 166–179.
13. Jeyaprakash, A.A., Klein, U.R., Lindner, D., Ebert, J., Nigg, E.A., and Conti, E. (2007). Structure of a Survivin-Borealin-INCENP core complex reveals how chromosomal passengers travel together. Cell *131*, 271–285.
14. Klein, U.R., Nigg, E.A., and Gruneberg, U. (2006). Centromere targeting of the chromosomal passenger complex requires a ternary subcomplex of Borealin, Survivin, and the N-terminal domain of INCENP. Mol. Biol. Cell *17*, 2547–2558.
15. Mackay, A.M., Eckley, D.M., Chue, C., and Earnshaw, W.C. (1993). Molecular analysis of the INCENPs (inner centromere proteins): separate domains are required for association with microtubules during interphase and with the central spindle during anaphase. J. Cell Biol. *123*, 373–385.
16. Ainsztein, A.M., Kandels-Lewis, S.E., Mackay, A.M., and Earnshaw, W.C. (1998). INCENP centromere and spindle targeting: identification of essential conserved motifs and involvement of heterochromatin protein HP1. J. Cell Biol. *143*, 1763–1774.
17. Vader, G., Kauw, J.J.W., Medema, R.H., and Lens, S.M.A. (2006). Survivin mediates targeting of the chromosomal passenger complex to the centromere and midbody. EMBO Rep. *7*, 85–92.
18. Bieling, P., Laan, L., Schek, H., Munteanu, E.L., Sandblad, L., Dogterom, M., Brunner, D., and Surrey, T. (2007). Reconstitution of a microtubule plus-end tracking system in vitro. Nature *450*, 1100–1105.
19. Mohan, R., Katrukha, E.A., Doodhi, H., Smal, I., Meijering, E., Kapitein, L.C., Steinmetz, M.O., and Akhmanova, A. (2013). End-binding proteins sensitize microtubules to the action of microtubule-targeting agents. Proc. Natl. Acad. Sci. USA *110*, 8900–8905.
20. Hooikaas, P.J., Martin, M., Mühlethaler, T., Kuijntjes, G.J., Peeters, C.A.E., Katrukha, E.A., Ferrari, L., Stucchi, R., Verhagen, D.G.F., van Riel, W.E., et al. (2019). MAP7 family proteins regulate kinesin-1 recruitment and activation. J. Cell Biol. *218*, 1298–1318.
21. Sessa, F., Mapelli, M., Ciferri, C., Tarricone, C., Areces, L.B., Schneider, T.R., Stukenberg, P.T., and Musacchio, A. (2005). Mechanism of aurora B activation by INCENP and inhibition by hesperadin. Mol. Cell *18*, 379–391.
22. Honda, R., Körner, R., and Nigg, E.A. (2003). Exploring the functional interactions between aurora B, INCENP, and survivin in mitosis. Mol. Biol. Cell *14*, 3325–3341.
23. Yue, Y., Blasius, T.L., Zhang, S., Jariwala, S., Walker, B., Grant, B.J., Cochran, J.C., and Verhey, K.J. (2018). Altered chemomechanical coupling causes impaired motility of the kinesin-4 motors KIF27 and KIF7. J. Cell Biol. *217*, 1319–1334.
24. Bieling, P., Telley, I.A., and Surrey, T. (2010). A minimal midzone protein module controls formation and length of antiparallel microtubule overlaps. Cell *142*, 420–432.
25. Monroy, B.Y., Sawyer, D.L., Ackermann, B.E., Borden, M.M., Tan, T.C., and Ori-McKenney, K.M. (2018). Competition between microtubule-associated proteins directs motor transport. Nat. Commun. *9*, 1487.
26. van Riel, W.E., Rai, A., Bianchi, S., Katrukha, E.A., Liu, Q., Heck, A.J., Hoogenraad, C.C., Steinmetz, M.O., Kapitein, L.C., and Akhmanova, A. (2017). Kinesin-4 KIF21B is a potent microtubule pausing factor. eLife *6*, e24746.
27. van der Vaart, B., van Riel, W.E., Doodhi, H., Kevenaar, J.T., Katrukha, E.A., Gumy, L., Bouchet, B.P., Grigoriev, I., Spangler, S.A., Yu, K.L., et al. (2013). CFEOM1-associated kinesin KIF21A is a cortical microtubule growth inhibitor. Dev. Cell *27*, 145–160.
28. Tseng, B.S., Tan, L., Kapoor, T.M., and Funabiki, H. (2010). Dual detection of chromosomes and microtubules by the chromosomal passenger complex drives spindle assembly. Dev. Cell *18*, 903–912.
29. van der Horst, A., Vromans, M.J.M., Bouwman, K., van der Waal, M.S., Hadders, M.A., and Lens, S.M.A. (2015). Inter-domain cooperation in INCENP promotes aurora B relocation from centromeres to microtubules. Cell Rep. *12*, 380–387.
30. Samejima, K., Platani, M., Wolny, M., Ogawa, H., Vargiu, G., Knight, P.J., Peckham, M., and Earnshaw, W.C. (2015). The inner centromere protein (INCENP) coil is a single α-helix (SAH) domain that binds directly to microtubules and is important for chromosome passenger complex (CPC) localization and function in mitosis. J. Biol. Chem. *290*, 21460–21472.
31. Wheatley, S.P., Kandels-Lewis, S.E., Adams, R.R., Ainsztein, A.M., and Earnshaw, W.C. (2001). INCENP binds directly to tubulin and requires

dynamic microtubules to target to the cleavage furrow. Exp. Cell Res. *262*, 122–127.

32. Trivedi, P., Zaytsev, A.V., Godzi, M., Ataullakhanov, F.I., Grishchuk, E.L., and Stukenberg, P.T. (2019). The binding of Borealin to microtubules underlies a tension independent kinetochore-microtubule error correction pathway. Nat. Commun. *10*, 682.
33. Verma, V., and Maresca, T.J. (2019). Microtubule plus-ends act as physical signaling hubs to activate RhoA during cytokinesis. eLife *8*, e38968.
34. Nakata, T., and Hirokawa, N. (1995). Point mutation of adenosine triphosphate-binding motif generated rigor kinesin that selectively blocks anterograde lysosome membrane transport. J. Cell Biol. *131*, 1039–1053.
35. Tcherniuk, S., Skoufias, D.A., Labriere, C., Rath, O., Gueritte, F., Guillou, C., and Kozielski, F. (2010). Relocation of aurora B and survivin from centromeres to the central spindle impaired by a kinesin-specific MKLP-2 inhibitor. Angew. Chem. Int. Ed. Engl. *49*, 8228–8231.
36. Mollinari, C., Kleman, J.P., Jiang, W., Schoehn, G., Hunter, T., and Margolis, R.L. (2002). PRC1 is a microtubule binding and bundling protein essential to maintain the mitotic spindle midzone. J. Cell Biol. *157*, 1175–1186.
37. Zhu, C., Lau, E., Schwarzenbacher, R., Bossy-Wetzel, E., and Jiang, W. (2006). Spatiotemporal control of spindle midzone formation by PRC1 in human cells. Proc. Natl. Acad. Sci. USA *103*, 6196–6201.
38. Pamula, M.C., Carlini, L., Forth, S., Verma, P., Suresh, S., Legant, W.R., Khodjakov, A., Betzig, E., and Kapoor, T.M. (2019). High-resolution imaging reveals how the spindle midzone impacts chromosome movement. J. Cell Biol. *218*, 2529–2544.
39. Guse, A., Mishima, M., and Glotzer, M. (2005). Phosphorylation of ZEN-4/MKLP1 by aurora B regulates completion of cytokinesis. Curr. Biol. *15*, 778–786.
40. Ahonen, L.J., Kukkonen, A.M., Pouwels, J., Bolton, M.A., Jingle, C.D., Stukenberg, P.T., and Kallio, M.J. (2009). Perturbation of Incenp function impedes anaphase chromatid movements and chromosomal passenger protein flux at centromeres. Chromosoma *118*, 71–84.
41. Montenegro Gouveia, S., Leslie, K., Kapitein, L.C., Buey, R.M., Grigoriev, I., Wagenbach, M., Smal, I., Meijering, E., Hoogenraad, C.C., Wordeman, L., et al. (2010). In vitro reconstitution of the functional interplay between MCAK and EB3 at microtubule plus ends. Curr. Biol. *20*, 1717–1722.
42. Perez-Riverol, Y., Csordas, A., Bai, J., Bernal-Llinares, M., Hewapathirana, S., Kundu, D.J., Inuganti, A., Griss, J., Mayer, G., Eisenacher, M., et al. (2019). The PRIDE database and related tools and resources in 2019: improving support for quantification data. Nucleic Acids Res. *47* (D1), D442–D450.
43. Uno, S.N., Kamiya, M., Yoshihara, T., Sugawara, K., Okabe, K., Tarhan, M.C., Fujita, H., Funatsu, T., Okada, Y., Tobita, S., and Urano, Y. (2014). A spontaneously blinking fluorophore based on intramolecular spirocyclization for live-cell super-resolution imaging. Nat. Chem. *6*, 681–689.
44. Vader, G., Cruijsen, C.W.A., van Harn, T., Vromans, M.J.M., Medema, R.H., and Lens, S.M.A. (2007). The chromosomal passenger complex controls spindle checkpoint function independent from its role in correcting microtubule kinetochore interactions. Mol. Biol. Cell *18*, 4553–4564.
45. Hengeveld, R.C.C., Hertz, N.T., Vromans, M.J.M., Zhang, C., Burlingame, A.L., Shokat, K.M., and Lens, S.M.A. (2012). Development of a chemical genetic approach for human aurora B kinase identifies novel substrates of the chromosomal passenger complex. Mol. Cell. Proteomics *11*, 47–59.
46. DeBonis, S., Skoufias, D.A., Lebeau, L., Lopez, R., Robin, G., Margolis, R.L., Wade, R.H., and Kozielski, F. (2004). In vitro screening for inhibitors of the human mitotic kinesin Eg5 with antimitotic and antitumor activities. Mol. Cancer Ther. *3*, 1079–1090.
47. Hill, E., Clarke, M., and Barr, F.A. (2000). The Rab6-binding kinesin, Rab6-KIFL, is required for cytokinesis. EMBO J. *19*, 5711–5719.
48. Kimura, M., Uchida, C., Takano, Y., Kitagawa, M., and Okano, Y. (2004). Cell cycle-dependent regulation of the human aurora B promoter. Biochem. Biophys. Res. Commun. *316*, 930–936.
49. Chang, J.L., Chen, T.H., Wang, C.F., Chiang, Y.H., Huang, Y.L., Wong, F.H., Chou, C.K., and Chen, C.M. (2006). Borealin/Dasra B is a cell cycle-regulated chromosomal passenger protein and its nuclear accumulation is linked to poor prognosis for human gastric cancer. Exp. Cell Res. *312*, 962–973.
50. Li, F., Ambrosini, G., Chu, E.Y., Plescia, J., Tognin, S., Marchisio, P.C., and Altieri, D.C. (1998). Control of apoptosis and mitotic spindle checkpoint by survivin. Nature *396*, 580–584.
51. Rappsilber, J., Mann, M., and Ishihama, Y. (2007). Protocol for micro-purification, enrichment, pre-fractionation and storage of peptides for proteomics using StageTips. Nat. Protoc. *2*, 1896–1906.
52. Yau, K.W., van Beuningen, S.F.B., Cunha-Ferreira, I., Cloin, B.M.C., van Battum, E.Y., Will, L., Schätzle, P., Tas, R.P., van Krugten, J., Katrukha, E.A., et al. (2014). Microtubule minus-end binding protein CAMSAP2 controls axon specification and dendrite development. Neuron *82*, 1058–1073.

STAR★METHODS

KEY RESOURCES TABLE

REAGENT or RESOURCE	SOURCE	IDENTIFIER
Antibodies		
rabbit anti-MKLP2	Bethyl (ITK)	Cat# A300-879A; RRID: AB_2779522
rabbit anti-Aurora B	Abcam	Cat# 2254-100; RRID: AB_302923
rabbit anti-Borealin	kind gift from Dr. S. Wheatley	N/A
rabbit anti-Survivin	R&D Systems	Cat# AF886; RRID: AB_355684
mouse anti-INCENP	Invitrogen	Cat# 39-2800; RRID: AB_2533405
rabbit anti-pH3S10	Upstate	Cat# 06-570; RRID: AB_310177
mouse anti-GFP	Roche	Cat# 11814460001; RRID: AB_390913
rabbit anti-PRC1	Santa Cruz	Cat# sc-8356; RRID: AB_2169665
rabbit anti-Anillin	kind gift from Dr. M. Glotzer	N/A
mouse anti-Aurora B	BD Transduction labs	Cat# 611083; RRID: AB_398396
goat anti-mouse HRP	Bio-Rad	Cat# 170-6516; RRID: AB_11125547
Goat anti-rabbit HRP	Bio-Rad	Cat# 170-6515; RRID: AB_11125142
Goat anti-mouse IgG Alexa488	Invitrogen	Cat# a11029; RRID: AB_2534088
Goat anti-rabbit IgG Alexa488	Invitrogen	Cat# a11034; RRID: AB_2576217
Goat anti-rabbit IgG Alexa568	Invitrogen	Cat# a11036; RRID: AB_10563566
Goat anti-mouse IgG Alexa568	Invitrogen	Cat# a11031; RRID: AB_144696
mouse anti-GST B14	Tebu	Cat# sc-138; RRID: AB_627677
Mouse anti-penta-His	QIAGEN	Cat# 34660; RRID: AB_2619735
GFP Booster ATTO-488	Chromotek	Cat# GBA488; RRID: AB_2631386
Alexa 568 Phalloidin	Life Technology	Cat# A12380
Bacterial and Virus Strains		
E. coli BL21(DE3)	Agilent	Cat# 200131
E. coli Rosetta2(DE3)	Novagen	Cat# 71400
Chemicals, Peptides, and Recombinant Proteins		
purified MKLP2-GFP-StrepII protein	This study	N/A
purified INCENP 1-100+linker+834-918-GFP-StrepII,Aurora B, Borealin, Survivin protein	This study	N/A
purified INCENP 1-100+linker+834-918-GFP-StrepII,Aurora B kinase dead, Borealin, Survivin protein	This study	N/A
purified MKLP2-mScarlet-StrepII protein	This study	N/A
StrepTactin Sepharose High Performance	GE Healthcare	Cat# GE28-9355-99
InstantBlue	Expedeon	Cat# SKU: ISB1L
HiPerfect Transfection Reagent	QIAGEN	Cat# 301705
X-tremeGENE 9 DNA Transfection Reagent	Roche	Cat# 06 365 809 001
Neutravidin	Invitrogen	Cat# A-2666
k-casein	Sigma	Cat# C0406
PLL-PEG-Biotin	Susos AG, Switzerland	Cat# PLL(20)-g[3.5]- PEG(2)/ PEG(3.4)- biotin(50%)
dithiothreitol	Sigma	Cat# R0861
Catalase	Sigma	Cat# C9322
Glucose oxidase	Sigma	Cat# G7141
GTP	Sigma	Cat# G8877
GMPCPP	Jena Biosciences	Cat# NU-405L
Tubulin Porcine Biotin	Cytoskeleton	Cat# T333P

(*Continued on next page*)

Continued

REAGENT or RESOURCE	SOURCE	IDENTIFIER
Tubulin Porcine TRITC	Cytoskeleton	Cat# TL590M
Tubulin Porcine	Cytoskeleton	Cat# T240-C
cOmplete , EDTA-free Protease Inhibitor Cocktail	Roche	Cat# 4693116001
Polyethyleneimine	Polysciences	Cat# 24765-2
RNase	Sigma	Cat# R6513
MNase	Sigma	Cat# n5386-500un
GFP-Trap beads agarose	Chromotek	Cat# gta-20
ultraglutamine	lonza	Cat# LO BE17-605E/U1
penicillin and streptomycin	Sigma	Cat# P0781-100ML
Blasticidin	InvivoGen	Cat# Ant-bl-5
Hygromycin B	Roche	Cat# 10843555001
doxycycline free FCS, Hyclone	GE Healthcare	Cat# SH30070.03T
Doxycycline	Sigma	Cat# D9891-1G
Thymidine	Sigma	Cat# T1895-25G
STLC	Tocris Bioscience	Cat# 2191/50
Okaidic acid	Roche	Cat# 11355554001
NP-40	Merck	Cat# 492016-100ML
sodium deoxycholate	Sial	Cat# D6750-25G
glycerol phosphoate	Sigma	Cat# G9422-10G
NaF	Sigma	Cat# S6776-100G
NaVO3	Sigma	Cat# S6508-10G
NaCl	Sigma	Cat# 71376-1KG
Triton X-100	Sigma	Cat# T9284
HEPES	Sigma	Cat# H3375-25G
Destiobiotin	IBA	Cat# 2-1000-002
ATP	Thermo	Cat# R0141
ZM447439	Tocris - R&D Systems	Cat# 2458/10
Histon H3	Roche Diagnostics	Cat# 11034758001
RO-3306	Calbiochem	Cat# 217699
TCEP	Sigma-Aldrich	Cat# 646547-10X1ml
Urea	Ambion	Cat# AM9902
ammonium bicarbonate	Sigma	Cat# 09830-1kg
Lys/C protease	Promega	Cat# V5117
purified INCENP 1-100+linker+834-918-mCherry-StrepII, Aurora B, Borealin, Survivin protein	This study	N/A
purified INCENP 1-100+linker+834-918-mCherry-StrepII, Aurora B kinase dead, Borealin, Survivin protein	This study	N/A
purified INCENP 1-100-GFP-StrepII, Borealin, Survivin protein	This study	N/A
purified INCENP 1-100-mCherry-StrepII, Borealin, Survivin protein	This study	N/A
Paprotrain	Millipore	Cat# 512533-25MG
Tween-20	VWR International	Cat# 8.22184.0500
ECL-HRP detection kit	Advanstra	Cat# K-12045-D20
ProLong anitfade	Molecular Probes	Cat# P36961
DMSO	Sigma	Cat# D5879-1L
purified GST	This study	N/A
purified GST-MKLP2 513-821	This study	N/A

(*Continued on next page*)

Continued

REAGENT or RESOURCE	SOURCE	IDENTIFIER
purified 6xHis-INCENP 1-100, Aurora B, Borealin, Survivin	This study	N/A
Glutathione Sepharose	GE Healthcare	Cat# 17-5132-01
Ni-NTA agarose	QIAGEN	Cat# 30230
Tris	Sigma-Aldrich	Cat# T1503
Glycerol	VWR Chemicals	Cat# 44448513
phenylmethanesulfonyl fluoride	Sigma-Aldrich	Cat# 78830
$ZnCl^2$	Merck	Cat# 8816.0250
D-(+)-Glucose	Sigma-Aldrich	Cat# G7528-1kg
Imidazole	Merck	Cat# 1.04716.1000
Isopropyl β-D-1-thiogalactopyranoside	Thermo Scientific	Cat# R0393
purified mCherry-EB3	[41]	N/A
purified T167N MKLP2-mScarlet-StrepII protein	This study	N/A
purified T167N MKLP2-GFP-StrepII protein	This study	N/A
HaloTag TMR ligand	Promega	Cat# 8252
Deposited Data		
The mass spectrometry proteomics data	ProteomeXchange Consortium via the PRIDE partner repository	PXD014665
Experimental Models: Cell Lines		
HEK239T	ATCC	N/A
HeLa FRT/TO	Kind gift from Dr. G. Kops	N/A
Oligonucleotides		
N/A	See Table S1 for oligonucleotides	N/A
Recombinant DNA		
plasmid pTT5 N1 eGFP StrepII	Novopro labs	Cat# V001466
plasmid pcDNA5/FRT/TO	Thermo Scientific	Cat# V652020
Plasmid pEGFP-N1	Clontech	Cat# 6085-1
pCR3	Invitrogen	N/A, discontinued
pOG044	Invitrogen	Cat# V600520
Plasmid pGEX-6P-1	GE Healthcare	Cat# 28-9546-48
Plasmid TUBB5-Halo	Addgene	Plasmid #64691
tri-cistronic pET28a vector containing 6xHis-INCENP 1-58, Aurora B, Borealin, Survivin	[32]	N/A
Software and Algorithms		
Graphpad Prism	Graphpad	https://www.graphpad.com/scientific-software/prism/
Fiji (ImageJ)	ImageJ	https://imagej.nih.gov/ij/
Metamorph	Molecular Devices	https://www.moleculardevices.com/products/cellular-imaging-systems/acquisition-and-analysis-software/metamorph-microscopy
		https://www.graphpad.com/scientific-software/prism/
KymoResliceWide plugin	Eugene Katrukha	https://github.com/ekatrukha/KymoResliceWide
DoM_Utrecht plugin	Eugene Katrukha	https://github.com/ekatrukha/DoM_Utrecht
MaxQuant 1.6.3.4	Max-Planck-Institute of Biochemistry	https://maxquant.org
Perseus	Max-Planck-Institute of Biochemistry	https://maxquant.org/perseus/
Clustal Omega	Conway Institute, University College Dublin	http://www.clustal.org/omega/

RESOURCE AVAILABILITY

Lead Contact

Information and requests for resources and reagents should be directed to and will be fulfilled by the Lead Contact, S.M.A. Lens (S.M.A.Lens@umcutrecht.nl).

Materials Availability

Plasmids and cell lines generated in this study can be obtained through the Lead Contact.

Data and Code Availability

The mass spectrometry proteomics data have been deposited to the ProteomeXchange Consortium via the PRIDE [42] partner repository with the dataset identifier PXD014665.

EXPERIMENTAL MODEL AND SUBJECT DETAILS

Cell lines and cell culture

HeLa Flp-In T-Rex (female) and human embryonic kidney 239T (HEK293T, female) cells were cultured in Dulbecco's modified Eagle's Medium (DMEM, Sigma-Aldrich) supplemented with 6% Fetal Calf Serum (FCS, Sigma-Aldrich), 2 mM UltraGlutamine (Lonza), 100 units/ml penicillin and 100 μg/ml Streptomycin (Sigma-Aldrich). HeLa Flp-In T-Rex cells were additionally supplemented with 4 μg/ml Blasticidin (PAA Laboratories). Cell lines were cultured at 37°C with 5% CO_2. Polyclonal HeLa Flp-In T-Rex cells with stable integration of GFP-tagged INCENP, GFP-tagged Borealin and GFP-tagged MKLP2 were cultured in the presence of 800 μg/ml Hygromycin B (Sigma-Aldrich) and 6% Tet-approved HyClone Fetal Bovine Serum (GE Healthcare). Protein expression was induced with 1 μg/ml of doxycycline (Sigma-Aldrich) for minimal 12 hr.

METHOD DETAILS

Plasmids

Full length MKLP2 (aa 1-890) was obtained by PCR from a human thymus cDNA library and was subsequently cloned into a pEGFP-N1 vector to generate MKLP2::GFP. This plasmid was used to generate the T167N MKLP2 mutant by site-directed mutagenesis, and to create the deletion mutants aa 1-513, aa 513-890, aa 513-821, aa 513-765 and aa 765-890 by PCR and restriction cloning into pEGFP-N1. MKLP2 deletion mutant aa 513-821, used for protein purification from *E. coli,* was inserted into a pGEX-6P-1 vector by PCR and restriction cloning. MKLP2 WT/T167N::GFP was cloned into a cDNA5/FRT/TO-hygromycin B vector (Invitrogen) for stable cell line production. Full length MKLP2 cDNA was also cloned into a pTT5 vector (Novopro labs) containing a C-terminal GFP::StrepII- or mScarlet::StrepII-tag used for protein purification. β-tubulin::Halo (TUBB5-Halo) was a gift from Yasushi Okada (Addgene plasmid # 64691; http://n2t.net/addgene:64691; RRID:Addgene_64691) [43].

Full length VSV-tagged INCENP, INCENP 49-918 (delta CEN-box) and INCENP d539-747 (deletion of single alpha helix, SAH) constructs were made as previously described [17, 29, 44]. Full length INCENP cDNA was used to generate the following INCENP fragments: aa 1-63, 1-100, 1-200 by PCR and restriction enzyme-based cloning into pEGFP-N1. Site directed mutagenesis was used to generate the INCENP mutant R35/36/39/40E. INCENP WT and INCENP R35/36/39/40E were subsequently cloned into a pcDNA5/FRT/TO-hygromycin B vector (Invitrogen) for stable cell line generation. INCENP (aa 1-100) and INCENP (aa 1-100) linker (GGGGS) INCENP (aa 834-918) were also cloned into a pTT5 vector (Novoprolabs) with a C-terminal GFP::StrepII- or mCherry::StrepII-tag for protein purification. A plasmid encoding full length Borealin (pCR3; Invitrogen), and previously described [17], was used as a template for site directed mutagenesis to generate the GFP::Borealin mutant R17/19E, K20E. The N-terminally GFP-tagged Borealin WT and Borealin R17/19E, K20E were subsequently cloned into a pcDNA5/FRT/TO-hygromycin B vector (Invitrogen) for stable cell line production. Full length Borealin, Survivin and Aurora B were amplified by PCR from previously described plasmids [17, 44, 45] and cloned into a pTT5 vector lacking GFP and StrepII coding DNA (Novoprolabs) and these were used for protein purification together with INCENP. The Aurora B (K106R), kinase dead, mutant was generated by site directed mutagenesis of pTT5-Aurora B. All newly generated plasmids were checked by DNA sequencing. Due to a point mutation in the stop codon of Aurora B K106R the protein has a short extension of 15 amino acids which is visible by western blot in Figure S2F. Finally, a tri-cistronic pET28a vector expressing 6xHis::INCENP1-58-Survivin-Borealin (gift from PT Stukenberg) was used for bacterial expression of the coreCPC after replacement of INCENP 1-58 for INCENP 1-100.

siRNA and plasmid transfection

HeLa Flp-In T-Rex cells were transfected with siRNAs for either INCENP (Dharmacon/3′UTR; GGCUUGGCCAGGUGUAUAUdTdT), MKLP2 (Dharmacon/3′UTR; CCACCUAUGUAAUCUCAUGdTdT) or Borealin (Dharmacon/3′-UTR; AGGUAGAGCUGUCUUCAdTdT) using HiPerfect Transfection Reagent (#301705; QIAGEN) and a standard HiPerfect transfection protocol with a 1:3 ratio for siRNA:-HiPerfect (37°C for 20 min) in Opti-MEM culture medium. The final concentration of siRNAs was 20 nM for siINCENP and siBorealin, and 40 nM for siMKLP2. Cells were analyzed 48 hr after siRNA transfection. Transient transfection of plasmids was performed with X-tremeGENE 9 DNA Transfection Reagent (Roche) according the manufacturer's protocol. To generate stable cell lines with

doxycyclin-inducible expression of wild-type (WT) or E35/36/39/40R INCENP::GFP; WT or R17/19E, K20E GFP::Borealin; or WT or T167N MKLP2::GFP, HeLa Flp-In T-Rex cells were co-transfected with pOG44 (Invitrogen) and pcDNA5/FRT/TO-hygromycin B plasmids encoding the indicated proteins. After transfection, cells were selected in medium supplemented with 800 μg/ml hygromycin B and 4 μg/ml blasticidin (Invitrogen). Polyclonal cell lines expressing the indicated GFP-tagged proteins were used for analysis. HEK293T cells were transfected with pTT5 plasmids using Polyethylenimine (PEI, Polysciences) with a 1:3 ratio for plasmid:PEI. Alternatively, HEK293T were transfected with pEGFP-N1 plasmids using a standard Calcium Phosphate transfection protocol.

Immunoprecipitation (IP)

HeLa Flp-In T-Rex cells were plated in 2.5 mM thymidine (Sigma-Aldrich) for 24 hr and released into 20 μM of the Eg5 inhibitor S-Trityl-L-Cysteine (STLC, Tocris Bioscience) [46] for 16 hr. Where indicated, doxycycline (1 μg/ml, Sigma-Aldrich) was added together with STLC to induce protein expression. HeLa Flp-In T-Rex cells or HEK293T cells transfected with plasmids encoding GFP-tagged MKLP2, INCENP and Borealin constructs were collected and washed twice in ice-cold PBS. Since endogenous CPC proteins and MKLP2 are poorly expressed in interphase [47–50], we enriched for mitotic cells by the addition of STLC. Cell pellets were lysed in lysis buffer (50 mM Tris-HCl, 150 mM NaCl, 0.5% NP-40, 0.1% sodium deoxycholate, 40 mM glycerol phosphate, 10mM NaF, 0.3 mM $NaVO_3$, 100 μM ATP, 100 μM $MgCl_2$, 100 nM okaidic acid and supplemented with protease inhibitors (Roche)) with 4 U/ml MNase (New England Biolabs) and 30 μg/ml RNase (Sigma-Aldrich). After clearing debris by centrifugation, a standard Bradford assay was performed to measure protein concentration, and cell lysates were incubated with 15 μl of GFP-Trap beads (Chromotek) for 2 hr at 4°C while rotating. Beads were washed three times with washing buffer (50 mM Tris-HCl, 400 mM NaCl, 0.5% NP-40, 0.1% sodium deoxycholate, 40 mM glycerol phosphate, 10 mM NaF, 0.3 mM $NaVO_3$, 100 μM ATP, 100 μM $MgCl_2$, 100 nM okaidic acid and supplemented with protease inhibitors (Roche)). Proteins were eluted by adding 20 μl of standard SDS sample buffer and by boiling the samples for 5 min. Samples were stored at −20°C until SDS-PAGE and western blotting.

Protein expression and pulldown from *E. coli*

For protein expression and purification from *E. coli*, BL21(DE3) cells were transformed with the respective GST-tagged constructs: GST control and GST::MKLP2(513-821). Bacteria were grown to an OD600 of 0.6-0.8 at 37°C, after which protein expression was induced with 0.1 mM Isopropyl β-d-1-thiogalactopyranoside (IPTG) for 20 hr at 25°C. Bacteria were spun down and subjected to one freeze-thaw cycle using liquid nitrogen to stimulate proper lysis. Bacteria were resuspended and sonicated on ice in cold lysis buffer containing 50 mM Tris pH 7.5, 300 mM NaCl, 5% glycerol, 0.5 mM DTT, 0.5 mM PMSF and Complete protease inhibitor cocktail (Roche). Lysates were centrifuged at ∼18.000 g for 60 min, and the supernatants were incubated with Glutathione Sepharose beads (GE Healthcare) for 4 hr at 4°C, followed by extensive washes on column with a wash buffer containing 50 mM Tris pH 7.5, 300 mM NaCl, 5% glycerol and 0.5 mM DTT. The glutathione beads containing GST (control) or GST::MKLP2(513-821) bound proteins were stored at 4°C and used for pulldown assay the same day.

For protein expression of CPC components from *E. coli*, Rosetta2(DE3) (Novagen) cells were transformed with a tricistronic pET28a vector containing 6 × His::INCENP 1–100 Survivin and Borealin. Bacteria were grown to an OD600 of ∼0.8 at at 37°C in LB supplemented with 60 mg l^{-1} $ZnCl_2$ and 0.2% glucose, after which protein expression was induced with 0.45 mM IPTG for 20 hr at 18°C. Bacteria were spun down and subjected to one freeze-thaw cycle using liquid nitrogen to stimulate proper lysis. Bacteria were resuspended and sonicated on ice in cold lysis buffer containing 50 mM Tris pH 7.5, 500 mM NaCl, 5% glycerol, 5 mM imidazole, 0.5 mM DTT, 0.5 mM PMSF and Complete protease inhibitor cocktail (Roche). Lysates were centrifuged at ∼18.000 g for 60 min and the supernatant was kept for the subsequent pulldown assay. The stored glutathione beads containing the GST-tagged proteins were incubated with the bacterial lysates containing the CPC components overnight at 4°C. The beads were washed with a wash buffer containing 50 mM Tris pH 7.5, 300 mM NaCl, 5% glycerol and 0.5 mM DTT. To visualize CPC components on Coomassie-stained SDS-PAGE gels, part of the CPC-containing supernatant was incubated with Ni-NTa beads (QIAGEN) for 2 hr at 4°C, followed by extensive washes on column with a wash buffer containing 50 mM Tris pH 7.5, 500 mM NaCl, 5% glycerol, 25 mM imidazole and 0.5 mM DTT. All pulldown beads and samples were supplemented with Laemmli sample buffer, boiled, and analyzed by SDS-PAGE and western blotting.

Protein purification and Aurora B kinase assay

HEK293T cells transfected with single (WT or T167N MKLP2::GFP::StrepII or WT or T167N MKLP2::mScarlett::StrepII) or multiple (coreCPC or miniCPC::GFP::StrepII or mCherry::StrepII, see Figure 2A) pTT5 plasmids were collected and washed twice in ice-cold PBS. Cells were lysed in ice-cold lysis buffer (50 mM HEPES, 300 mM NaCl, 0.5% Triton X-100, pH 7.4) supplemented with protease inhibitors (Roche). After clearing debris by centrifugation at 4°C, cell lysates were incubated with StrepTactin beads (StrepTactin Sepharose High Performance, GE Healthcare) for one hour at 4°C. Beads were washed three times with ice cold washing buffer (50 mM HEPES, 150 mM NaCl, 0.01% Triton X-100). For MKLP2 proteins, beads were washed an additional time with a high salt wash buffer (1M NaCl). The proteins were subsequently eluted in elution buffer (50 mM HEPES, 150 mM NaCl, 0.01% Triton X-100 and 2.5 mM desthiobiotin) for 10 min. Protein concentration was determined by SDS-PAGE and Coomassie Blue staining using InstantBlue (Expedeon), using purified BSA titration as a reference. Purified proteins were snap-frozen and stored at −80°C. A kinase assay was performed by adding 5 μg of purified miniCPC with either Aurora B WT or KD, into a reaction mixture containing kinase buffer (10 mM $MgCl_2$, 25 mM HEPES pH 7.5, 25 mM β-glycerophosphate, 0.5 mM DTT, 0.5 mM vanadate, 100 μM ATP),

and 0.2 mg/ml Histone H3 as substrate (Roche Diagnostics). Either DMSO or 2 μM Aurora B inhibitor (ZM447439, Tocris) was added to the reaction as well. After 30 min incubation at 30°C, the reaction was stopped by the addition of sample buffer. Samples were analyzed by western blot using a primary antibody specific for phosphorylated Serine 10 in Histone H3 (H3S10ph).

Western blotting

Mitotic HeLa or transfected HEK293T cells were collected and lysed in standard Laemmli buffer. Protein concentration was determined using a Lowry assay. Protein samples of either whole cell extracts, bacterial lysates or IP's were separated by SDS-PAGE and transferred to nitrocellulose membranes. Membranes were blocked in 4% milk in Tris-buffered saline containing 0.5% Tween-20 (TBST) and subsequently incubated with a primary antibody for 2 hr. Primary antibodies used were rabbit anti-MKLP2 (Bethyl (ITK) A300-879A), rabbit anti-Aurora B (Abcam 2254-100), rabbit anti-Borealin (gift from Dr. S. Wheatley), rabbit anti-Survivin (R&D Systems AF886), mouse anti-INCENP (Invitrogen 39-2800), rabbit anti-H3S10ph (Upstate 06-570), mouse anti-α-tubulin (Sigma, T5168), mouse anti-GFP (Roche 11814460001), mouse anti-GST B14 (Tebu SC-138), and mouse anti-penta-His (QIAGEN 34660). Membranes were washed three times with TBST, and subsequently incubated with goat anti-mouse or anti-rabbit horseradish peroxidase (HRP)-conjugated secondary antibodies (Bio-Rad). An ECL chemiluminescence detection kit (GE Healthcare) was used to visualize the protein-antibody complex.

Mass spectrometry

Eluted MKLP2::GFP::StrepII or GFP::StrepII samples (three technical replicates of each) were first denatured and alkylated by adding alkylation buffer (10 mM tris(2-carboxyethyl)phosphine (TCEP), 40 mM 2-chloroacetamide (CAA), 8 M urea, 1 M ammonium bicarbonate. After 30 min of incubation the samples were diluted fourfold with 1 M ammonium bicarbonate and 250 ng Trypsin/Lys-C protease (Promega) was added and followed by overnight digestion at 37°C on a shaker. The samples were then cleaned up using homemade C18 stagetips [51], and a quarter was used for the analysis with LC-MS (Thermo Easy-nLC 1000, Thermo Orbitrap Fusion Tribrid) running a 140 min gradient (300 nl/min, 30 cm, 1.9 μm C18 column) with 240k (at 200 m/z) full MS resolution and a 1 s MS2 duty cycle (top speed, highest to low intensity, HCD fragmentation). Raw files were analyzed with Maxquant software, version 1.6.3.4. For identification, the Human Uniprot database was searched with oxidation of and carbamidomethylation of cysteine set as fixed modification, while peptide and protein false discovery rates were set to 1%. The median intensity of the iBAQ values was then plotted as Log2 transformed values with a red line (x = 0) and a green line (x+5) added as visual aid.

Immunofluorescence microscopy

For immunofluorescence (IF) of anaphase cells, HeLa Flp-In T-Rex cells were plated in 2.5 mM thymidine (Sigma-Aldrich) for 24 hr in 24 well plates containing 12 mm High Precision coverslips (Superior-Marienfeld GmbH & Co) and subsequently released into medium containing 5 μM Cdk1 inhibitor RO3306 (Calbiochem) for another 16 hr to synchronize cells in G2. Where indicated, doxycycline (1 μg/ml, Sigma-Aldrich) was added together with RO3306 to induce protein expression. Cells were released from the RO3306-induced G2 block by washing three times with warm medium. Where indicated, 50 μM Paprotrain (Millipore) was added 50 min after the release from the Cdk1 inhibitor. After 10 min, cells were processed for IF. To identify binucleates, cells were released from Cdk1 inhibitor, Paprotrain was added 50 min after the release and cells were fixed 24 hr after release. Cells were fixed with 4% PFA in PBS for 7 min and permeabilized in 0.25% Triton X-100 in PBS for 5 min. Cells were blocked in PBS containing 3% BSA and 0.1% Tween-20. Primary antibodies used were: rabbit anti-MKLP2 (Bethyl (ITK) A300-878A), rabbit anti-PRC1 (Santa Cruz sc-8356), mouse anti-Aurora B (BD Transduction labs 611083), rabbit anti-Anillin (a kind gift from Michael Glotzer) and mouse anti-GFP (Roche 11-814-460-001) or GFP booster ATTO-488 (Chromotec GBA488). Secondary antibodies used were: goat anti-mouse or goat anti-rabbit IgG-Alexa 488, goat anti-mouse or goat anti-rabbit IgG-Alexa 568 (Invitrogen). 4',6-Diamidino-2-Phenylindole (DAPI, Sigma-Aldrich) was used for DNA staining. Phalloidin-Alexa 568 (Invitrogen, A12380) was used to visualize F-actin to facilitate scoring of binucleates. Coverslips were mounted in ProLong Antifade (Molecular Probes). Images were taken with a Personal DeltaVision system (Applied Precision) equipped with a 100x / NA 1.40 UPLS Apo-UIS2 objective (Olympus) and a CoolSNAP HQ CCD camera (Photometrics). Images were deconvolved in Softworx. For each experiment, all images were acquired with identical illumination settings. Images are projections of deconvolved Z stacks, unless stated otherwise.

In vitro microtubule dynamics assays

Doubly cycled GMPCPP microtubule seeds were prepared as described before [19], by incubating a tubulin mix containing 70% unlabeled porcine brain tubulin (Cytoskeleton), 18% biotin-tubulin (Cytoskeleton) and 12% rhodamine-tubulin (Cytoskeleton) at a total final tubulin concentration of 20 μM with 1 mM GMPCPP (Jena Biosciences) at 37°C for 30 min. Microtubules were pelleted by centrifugation in an Airfuge for 5 min at 119,000 × g and then depolymerized on ice for 20 min. This was followed by a second round of polymerization at 37°C with 1 mM GMPCPP. microtubule seeds were then pelleted as above and diluted in MRB80 buffer containing 10% glycerol, snap frozen in liquid nitrogen and stored at −80°C.

Flow chambers, assembled from sticking plasma-cleaned glass coverslips onto microscopic slides with a double sided tape were functionalized by sequential incubation with 0.2 mg/ml PLL-PEG-biotin (Susos AG, Switzerland) and 1 mg/ml NeutrAvidin (Invitrogen) in MRB80 buffer (80 mM piperazine-N,N[prime]-bis(2-ethanesulfonic acid), pH 6.8, supplemented with 4 mM $MgCl_2$, and 1 mM EGTA. microtubule seeds were attached to the coverslip through biotin-NeutrAvidin interactions. Flow chambers were further blocked with 1 mg/ml κ-casein (Sigma-Aldrich). The *in vitro* reaction mixture consisted of 18 μM tubulin, 50 mM KCl, 0.1%

methylcellulose, 0.5 mg/ml κ-casein, 1 mM GTP, an oxygen scavenging system (20 mM glucose, 200 μg/ml catalase, 400 μg/ml glucose-oxidase, and 4 mM DTT), 2 mM ATP, MKLP2 motors at indicated concentrations (concentrations were calculated for monomeric proteins), and CPC protein complexes at indicated concentrations. After centrifugation in an Airfuge for 5 min at 119,000 x g, the reaction mixture was added to the flow chamber containing the microtubule seeds and sealed with vacuum grease. The experiments were conducted at 30°C, and data were collected using total internal reflection fluorescence (TIRF) microscopy. For most experiments, the reaction mixture was composed of 17.5 μM tubulin supplemented with 0.5 μM rhodamine-labeled tubulin to properly visualize microtubules in the assay. For assays where we labeled growing microtubule ends, bacterial purified mCherry::EB3 [41] was added to the assay at a concentration of 20 nM. All tubulin products were purchased from Cytoskeleton Inc.

TIRF Microscopy

In vitro reconstitution assays were imaged on a TIRF microscope setup as described previously [19] or on an ILAS-2 TIRF setup. The former system consisted of an inverted research microscope Nikon Eclipse Ti-E (Nikon) with the perfect focus system (Nikon), equipped with Nikon CFI Apo TIRF 100x 1.49 N.A. oil objective (Nikon) and controlled with MetaMorph 7.7.5 software (Molecular Devices). The microscope was equipped with TIRF-E motorized TIRF illuminator modified by Roper Scientific France/PICT-IBiSA, Institut Curie. To keep the *in vitro* samples at 30°C, a stage top incubator model INUBG2E-ZILCS (Tokai Hit) was used. For excitation, 491 nm 100 mW Calypso (Cobolt) and 561 nm 100 mW Jive (Cobolt) lasers were used. We used ET-GFP 49002 filter set (Chroma) for imaging of proteins tagged with GFP or ET-mCherry 49008 filter set (Chroma) for imaging of rhodamine-labeled tubulin or proteins tagged with mScarlet or mCherry. For simultaneous imaging of green and red fluorescence, we used an Evolve512 EMCCD camera (Photometrics) and ET-GFP/mCherry filter cube (59022; Chroma) together with an Optosplit III beamsplitter (Cairn Research Ltd) equipped with double-emission filter cube configured with ET525/50 m, ET9630/75 m and T585lprx (Chroma). Fluorescence was detected using an EMCCD Evolve 512 camera (Roper Scientific) with the intermediate lens 2.5X (Nikon C mount adaptor 2.5X). The final magnification using EMCCD camera was 0.063 μm/pixel.

ILAS-2 system (Roper Scientific, Evry, France) is a dual laser illuminator for azimuthal spinning TIRF (or Hilo) illumination and with a custom modification for targeted photomanipulation. This system was installed on Nikon Ti microscope (with the perfect focus system, Nikon), equipped with 150 mW 488 nm laser and 100 mW 561 nm laser, 49002 and 49008 Chroma filter sets. For simultaneous imaging of green and red fluorescence, we used an Evolve512 EMCCD camera (Photometrics) and ET-GFP/mCherry filter cube (59022; Chroma) together with an Optosplit III beamsplitter (Cairn Research Ltd) equipped with double-emission filter cube configured with ET525/50 m, ET9630/75 m and T585lprx (Chroma). Fluorescence was detected using an EMCCD Evolve mono FW DELTA 512x512 camera (Roper Scientific) with the intermediate lens 2.5X (Nikon C mount adaptor 2.5X). The setup was controlled with MetaMorph 7.8.8 software (Molecular Device). To keep the *in vitro* samples at 30°C, a stage top incubator model INUBG2E-ZILCS (Tokai Hit) was used. The final resolution using EMCCD camera was 0.065 μm/pixel.

Single-molecule intensity analysis

Sample preparation for the fluorescence intensity analysis was performed by immobilizing diluted GFP or MKLP2::GFP full length proteins non-specifically to the plasma cleaned glass coverslips in flow chambers. After protein addition, the flow chambers were washed with MRB80 buffer, sealed with vacuum grease and immediately imaged with a TIRF microscope. Approximately 10 images of previously unexposed coverslip areas were acquired. GFP and MKLP2::GFP full length proteins were located in different chambers of the same coverslip, so identical imaging conditions could be preserved. All acquisitions were obtained under identical laser power, exposure time and TIRF angle.

Live cell microscopy

Imaging of MKLP2::GFP and INCENP::GFP in HeLa Flp-In T-Rex cells was done in Lab-tek (8 well, Chambered Coverglass W/Cover #1.5 Borosilicate Sterile, Thermo Fisher Scientific). Cells were blocked in late G2 by overnight Cdk1 inhibition (RO-3306) and released prior to imaging by 3x washing with Leibovitz's medium (Sigma-Aldrich). DMSO or Paprotrain was added 20 min after release from the Cdk1 inhibition. To visualize microtubules, MKLP2::GFP expressing HeLa cells were transfected with a β-tubulin::Halo construct. To label the expressed β-tubulin::Halo, the imaging medium was supplemented with cell-permeable HaloTag TMR Ligand (Promega) 30 min prior to imaging. Medium was changed to Leibovitz's medium (Sigma-Aldrich) supplemented with 10% FCS (FBS, Sigma-Aldrich), 2 mM UltraGlutamine (Lonza) and 100 units/ml penicillin and 100 μg/ml streptomycin (Sigma-Aldrich).

Spinning disk microscopy was performed on inverted research microscope Nikon Eclipse Ti-E (Nikon), equipped with the perfect focus system (Nikon), Plan Apo VC 100x N.A. 1.40 oil objective (Nikon), spinning disk Yokogawa CSU-X1-A1 with 405-491-561-642 quad-band mirror (Yokogawa). The system was also equipped with ASI motorized stage with the piezo plate MS-2000-XYZ (ASI), Back-Illuminated Evolve 512 EMCCD camera (Photometrics) or Back-Illuminated Prime BSI sCMOS camera (Photometrics) and controlled by the MetaMorph 7.10 software (Molecular Devices). 491nm 100mW Calypso (Cobolt), 561nm 100mW Jive (Cobolt) and 642 nm 110 mW Stradus (Vortran) lasers were used as the light sources. ET-GFP filter set (49002, Chroma) was used for imaging of proteins tagged with green fluorescent marker; ET-mCherry filter set (49008, Chroma) was used for imaging of proteins tagged with red fluorescent marker, ET-Cy5 filter set (49006, Chroma) was used for imaging of proteins tagged with far-red fluorescent marker. For simultaneous imaging of green and red fluorescence we used ET-GFP/mCherry filter set (59022, Chroma) together with DualView DV2 beam splitter (Photometrics). 16-bit images were projected onto the Evolve 512 EMCCD camera with intermediate lens 2.0X (Edmund Optics) at a magnification of 0.066 μm/pixel or onto Prime BSI sCMOS camera with no intermediate

lens at a magnification of 0.063 μm/pixel. To keep cells at 37°C we used stage top incubator (model INUBG2E-ZILCS, Tokai Hit). Imaging of INCENP::GFP in HeLa Flp-In T-Rex cells with or without Paprotrain (50 μM) was performed on a Spinning Disk Microscope consisting of an inverted research microscope Eclipse Ti2-E (Nikon), equipped with the Perfect Focus System (Nikon), CFI Plan Apo TIRF 60X oil objective (Nikon), spinning disk Yokogawa CSU-W1-T2. The system was also equipped with a Ti2-S-SE-E motorized stage (Nikon) and the piezo insert NANO Z200-N2 (Mad City Labs), environmental chamber for temperature (37°C) and CO_2 control (OkoLab) and fully controlled with NIS-Elements-AR_v5.20 software (Nikon). Using the 405-488-568-647quad-band Ex mirror (Yokogawa) in combination with the 561nm 100mW (Oxxius) laser as the light source, the Em-filter 525/50 nm BrightLine (FF03-525/50-25, Semrock) and the Zyla 4.2 Plus sCMOS camera (Andor) we were able to detect INCENP::GFP.

QUANTIFICATION AND STATISTICAL ANALYSIS

Single molecule GFP counting assays

ImageJ plugin Comdet v.0.3.61 and DoM_Utrecht v1.1.1.5 (https://github.com/ekatrukha/DoM_Utrecht) were used for detection and fitting of single molecule fluorescent spots as described previously [52]. With this method, individual spots were fitted with 2D Gaussian, and the amplitude of the fitted Gaussian function was used as a measure of the fluorescence intensity value of an individual spot. These fitted peak intensity values were used to build fluorescence intensity histograms which could be fitted to a Gaussian curve using GraphPad Prism 7.

Analysis of *in vitro* reconstitution data

Images and videos were processed and analyzed with Fiji image processing software (ImageJ). Maximum intensity projections were made using z projection. Kinesin velocities, run lengths and landing frequencies were obtained from kymograph analysis using ImageJ plugin KymoReslideWide v.0.4 (https://github.com/ekatrukha/KymoResliceWide). Kinesin parameters were quantified for processive events that last > 1 s. Static events were not included in velocity and run length quantifications. Quantification of landing frequencies was corrected for microtubule length, time of acquisition and kinesin concentration. Processive events were quantified and subdivided into "complete" and "incomplete" tracks. Tracks where both kinesin landing and detachment were observed were defined as complete, whereas incomplete tracks were tracks that exceeded the 90 s acquisition time or partially took place outside of the acquisition area. In cases of hyperprocessive events (imaging of miniCPC::GFP, or MKLP2::GFP in the presence of miniCPC) with many incomplete tracks, the observed event frequency per microtubule was quantified instead of landing frequency. Again, these data were corrected for microtubule length, time of acquisition and kinesin or CPC concentration. To distinguish directional and processive CPC events from diffusively behaving particles, only unidirectional events with a duration > 2.5 s were quantified. CPC::GFP labeling intensities on *in vitro* polymerized dynamic microtubules were measured from 2 pixel wide line scans along microtubules. An adjacent line scan 10 pixels away from the same microtubule was used as a background intensity measurement. microtubule labeling intensity was corrected by subtraction of this background intensity measurement. Imaging conditions were kept identical for all samples in the same experiment.

For *in vitro* experiments with Paprotrain or the T167N mutant motor, kinesin dwell time and landing frequency were quantified for all events that last > 1 s. For the *in vitro* experiments with Paprotrain, runs with a velocity < 0.025 μm/s were classified as static events. The percentage of static events per microtubule was quantified as a percentage of all kinesin events per microtubule. In the experiments with Paprotrain, non-motile (static) events were included in velocity and run length quantifications. Kinesins running on GMPCPP microtubule seeds were excluded as much as possible from the analysis.

Analysis of live cell imaging data

Image analysis was performed with Fiji image processing software (ImageJ). MKLP2 and INCENP velocities were obtained from kymograph analysis using ImageJ plugin KymoReslideWide v.0.4 (https://github.com/ekatrukha/KymoResliceWide). To distinguish directional MKLP2::GFP and INCENP::GFP events in cells from diffusive or statically behaving particles, only unidirectional events with a relatively constant velocity > 0.05 μm/s and a duration > 2.5 s were quantified. In addition, only events that could be measured using a kymograph were quantified in these experiments.

Quantification of immunofluorescence

Images were deconvolved in Softworx (Applied Precision). For each experiment, all images were acquired with identical illumination settings. Images are projections of deconvolved z stacks. Image analysis was performed with Fiji image processing software (ImageJ). To quantify and compare the mean fluorescence intensities (MFIs) of Aurora B on the equatorial cortex (marked by Anillin), the spindle midzone (marked by PRC1), and on chromatin (DAPI), a regions of interest (ROIs) were made on the basis of Anillin, PRC1 or DAPI localization. A random region of the cytoplasm was used as background measurement, and background intensity per cell was subtracted from the fluorescence intensity measured in the indicated ROIs. Line plots were performed with Fiji image processing software (ImageJ) and visualized in Graphpad Prism 7 software.

Protein sequence alignment

Protein sequences from several kinesin families were retrieved from Uniprot: kinesin-1, KIF5B (UniProt: P33176); kinesin-2, KIF17 (UniProt: Q9P2E2); kinesin-3, KIF1A (UniProt: Q12756); kinesin-4, KIF4A (UniProt: O95239); kinesin-5, KIF11 (Eg5)

(UniProt: P52732); kinesin-6, KIF20A (MKLP2) (UniProt: O95235); kinesin-6, KIF20B (MPP-1) (UniProt: Q96Q89); kinesin-6, KIF23 (MKLP1) (UniProt: Q02241). These sequences were aligned and analyzed online using ClustalOmega software.

Statistical analysis

Statistical significance was analyzed either using the Mann-Whitney *U* test, or t test, as indicated in the figure legends. For the t tests, data distribution was checked for normal distribution of the data. Kinesin and CPC velocities are represented using frequency distributions and Gaussian curve fits. For this fitting, data distributions were assumed to be normal, but this was not formally tested. Statistical analysis was performed with Graphpad Prism 7 or Prism 8 software.